
Solar coronal plumes and the fast solar wind

Bhola N. Dwivedi • Klaus Wilhelm

Abstract The spectral profiles of the coronal Ne VIII line at 77 nm have different shapes in quiet-Sun regions and coronal holes (CHs). A single Gaussian fit of the line profile provides an adequate approximation in quiet-Sun areas, whereas a strong shoulder on the long-wavelength side is a systematic feature in CHs. Although this has been noticed since 1999, no physical reason for the peculiar shape could be given. In an attempt to identify the cause of this peculiarity, we address three problems that could not be conclusively resolved in a review article by a study team of the International Space Science Institute (ISSI; Wilhelm et al. 2011): (1) The physical processes operating at the base and inside of plumes as well as their interaction with the solar wind (SW). (2) The possible contribution of plume plasma to the fast SW streams. (3) The signature of the first-ionization potential (FIP) effect between plumes and inter-plume regions (IPRs). Before the spectroscopic peculiarities in IPRs and plumes in polar coronal holes (PCHs) can be further investigated with the instrument Solar Ultraviolet Measurements of Emitted Radiation (SUMER) aboard the Solar and Heliospheric Observatory (SOHO), it is mandatory to summarize the results of the review to place the spectroscopic observations into context. Finally, a plume model is proposed that satisfactorily explains the plasma flows up and down the plume field lines and leads to the shape of the neon line in PCHs.

Keywords Sun: corona – solar wind – UV radiation

Bhola N. Dwivedi

Department of Physics, Indian Institute of Technology (Banaras Hindu University), Varanasi-221005, India
 bholadwivedi@gmail.com

Klaus Wilhelm

Max-Planck-Institut für Sonnensystemforschung (MPS), 37077 Göttingen, Germany
 wilhelm@mps.mpg.de

1 Introduction

In a recent review (Wilhelm et al. 2011), many aspects of the solar coronal plume phenomenon have been presented. In most cases the authors of the review, members of a study team of the International Space Science Institute (ISSI), Bern, arrived at conclusive results. However, some open points remained, of which we consider three. They have been formulated with the abbreviations IPR (inter-plume region), SW (solar wind), and FIP (first-ionization potential):

- Although models of plumes and their formation are available, an exact description of the physical processes operating at the base and inside of plumes as well as their interaction with the SW is still outstanding.
- Is there any contribution of plume plasma to the fast SW streams at all?
- What produces the clear FIP effect signature between plumes and IPRs?

In this paper, we propose – based on observational data – tentative solutions in these problem areas.

Earlier review papers on plumes have been published as well, and we refer the reader to them for a general introduction to this solar phenomenon (e.g., van de Hulst 1950; Saito 1965; Newkirk and Harvey 1968; DeForest et al. 1997). Nevertheless, it is necessary to list some of the basic properties of plumes and IPR as they are known at present from observations described by Wilhelm et al. (2011) and references therein: Polar plumes delineate magnetic field lines of the minimum corona in PCHs and expand super-radially in the low β -regime of the corona as can be seen from Fig. 1. Plumes observed in WL (white light) and VUV (vacuum ultraviolet) result from plasma density enhancements in CHs. The electron density ratio between plumes and IPRs is between three and seven in the

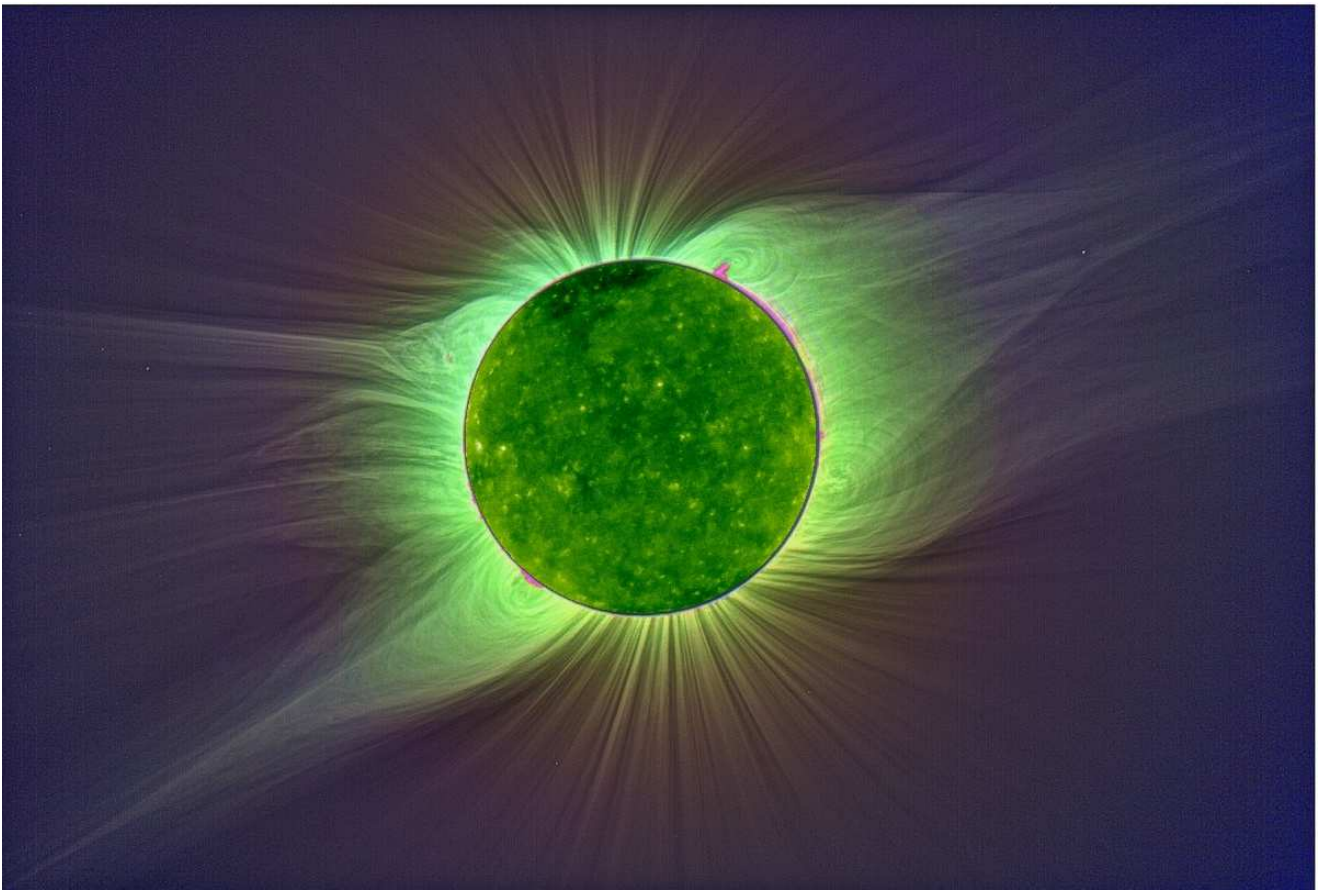


Fig. 1 The solar corona during the total eclipse on 1 August 2008 observed from Mongolia. The corona at solar minimum conditions has wide PCHs with reduced radiation, open magnetic field lines and many plume structures. At lower latitudes closed field-line regions dominate the corona and extend into coronal streamers (from Pasachoff et al. 2009, composite eclipse image by M. Druckmüller, P. Aniol and V. Rušin). An image in 19.5 nm of the solar disk taken from the Extreme ultraviolet Imaging Telescope (EIT) (Delaboudinière et al. 1995) on SOHO at the time of the eclipse has been inserted into the shadow of the Moon (Wilhelm et al. 2011).

low corona and decreases at greater heights. The electron temperature in plumes is $T_e \leq 1$ MK. In IPRs it is higher by ≈ 0.2 MK with a tendency of even higher values at greater heights. A plume shows some evolution during its lifetime. Footpoints of beam plumes lie near magnetic flux concentrations interacting with small magnetic dipoles. The reconnection activity generates heat near the base of a plume and leads to jets that probably provide some of the plume plasma. The SW outflow velocity is higher in IPRs than in plumes. Plumes and IPRs have a distinctly different abundance composition, in the sense that the ratio of low-FIP/high-FIP elements is much larger in plumes than in IPRs. Rosettes in the chromospheric network could be of importance for the plume formation.

The following definition has been used for β :

$$\frac{p}{p_{\text{mag}}} = \frac{n k_B T}{(B^2/2\mu_0)} = \beta, \quad (1)$$

where p is the plasma pressure and p_{mag} is the magnetic pressure with n the particle density, k_B the Boltzmann constant, T the plasma temperature, B the magnetic flux density, and μ_0 the vacuum permeability.

The plasma of PCHs is optically thin for VUV lines. Nevertheless, it was possible to identify two different plasma regimes, plumes and IPR, by studying density- and temperature-sensitive line ratios (Wilhelm 2006). From EIT observations, Gabriel et al. (2003) have found that plumes must occur with two different morphologies, beam plumes and curtain or network plumes, because the latter appear to be aligned along network lanes. Network plumes, and probably beam plumes, are composed of individual micro-plumes (Gabriel et al. 2009). This aspect was further studied by de Patoul et al. (2013) who found typical beam plumes with a localized cross-section and those with an elongated cross-section as expected for network plumes.

Their tomography results show that intermediate configurations also exist.

Fig. 1 clearly shows that the field lines of a PCH open into interplanetary space. The observations of the spacecraft Ulysses demonstrate that on these field lines the fast solar wind escapes from the Sun with asymptotic speeds of approximately 800 km s^{-1} (cf., e.g., Woch et al. 1997; McComas et al. 2000).

2 The neon emission line near 77 nm

The transition $2s^2S_{1/2} - 2p^2P_{3/2}$ in the Ne^{7+} ion leads to a prominent solar emission line in the Ne VIII spectrum near 77 nm. The spectroscopic observations of this line are of major importance in this study and therefore some background information might be helpful. The first wavelength determination $\lambda_0 = 77.042 \text{ nm}$ with a standard uncertainty of 0.003 nm was performed in the laboratory by Fawcett et al. (1961). The large Doppler width of the line emitted from high-temperature plasmas limits the accuracy of such measurements. Solar observations, therefore, provide the best values of the rest wavelength in vacuum $\lambda_0 = (77.0428 \pm 0.0003) \text{ nm}$ (Damasch et al. 1999). The Ne VIII line is formed at an electron temperature of 620 000 K (cf., Wilhelm et al. 2002). The contribution function has a long tail towards higher temperatures typical for lithium-like ions. The line is thus ideally suited for studies of the upper transition region and its interface with the *low corona*. Measurements of Doppler shifts of this line in quiet-Sun (QS) regions initially provided inconsistent results for the average shift. The problems were, however, related to the inaccurate knowledge of the vacuum rest wavelength (Doschek et al. 1976; Hassler et al. 1991; Brekke et al. 1997; Chae et al. 1997). Later studies showed an average blue shift of $\approx 1 \text{ km s}^{-1}$ in QS regions (Peter and Judge 1999; Damasch et al. 1999), and a more pronounced average blue shift of $\approx 6 \text{ km s}^{-1}$ in PCHs.

3 Observed outflow speeds in polar coronal holes

Before an attempt can be undertaken to answer the question: *Are there plume signatures in the fast solar wind?* the observed outflow speeds in plumes and IPR have to be considered as well as the elemental composition of the solar photosphere and the polar corona.

Strong outflows were observed by Hassler et al. (1999) in a PCH above bright areas as seen in the Si II

153.3 nm line at the intersections of chromospheric network lanes. However, these areas are rather dark in the Ne VIII radiance maps and have a typical flow component of Ne^{7+} ions of 10 km s^{-1} along the line of sight. The ion outflow speed can then be obtained with the magnetic field model of Banaszekiewicz et al. (1998) as 14 km s^{-1} . No outflow is observed in BPs at the base of polar plumes (Wilhelm et al. 2000).

Funnel-shaped magnetic flux tubes from the photosphere to the corona are typical features in PCHs (cf., e.g., Gabriel 1976; Tu et al. 2005; Ito et al. 2010). These funnels are seen as source regions of the fast SW, but they can also contain coronal plumes. One funnel analysed by Tu et al. (2005) in their Figs. 1(F) and 4 at $x = 50''$ and $y = 175''$ does not show any outflow speed. It had earlier been identified as a plume (Wilhelm et al. 2000). Two plumes seen by Hassler et al. (1999) also appear to be stationary.

Outflow speeds observed in PCHs by many researchers have been compiled by Wilhelm et al. (2011) and are included here in Fig. 2 together with the escape velocities at heliocentric distances, R :

$$V_F(R) = \sqrt{\frac{2 G_N M_\odot}{R}}, \quad (2)$$

where G_N is the gravitational constant and M_\odot the mass of the Sun. The speeds measured in IPRs and PCHs (without distinction between IPRs and plumes, which have a small filling factor) increase with increasing heliocentric distance without too much scatter and attain escape velocities near $R = 3 R_\odot$, whereas the speeds published for plumes vary considerably and nowhere reach the escape velocity. We argue that there are probably two reasons for the high variability: (1) Plumes evolve during their lifetime and may display different characteristics at different stages. (2) Jets with high outflow speeds are often observed near the footpoints of plumes (e.g., Raouafi et al. 2008; de Patoul et al. 2013; Raouafi & Stenborg 2014).

This is in line with a suggestion by van de Hulst (1950) that plumes are rather static with occasional plasma injections along the field lines. This has been confirmed by the findings of Sheeley et al. (1997) that the direction of time is easy to see with the Large Angle Spectroscopic Coronagraph (LASCO) on SOHO by tracing lateral inhomogeneities in coronal streamers, but difficult to identify over PCHs.

4 First-Ionization Potential effects in the solar atmosphere and the solar wind

In the corona, the abundances of elements with respect to the photosphere vary and the FIP effect plays a dom-

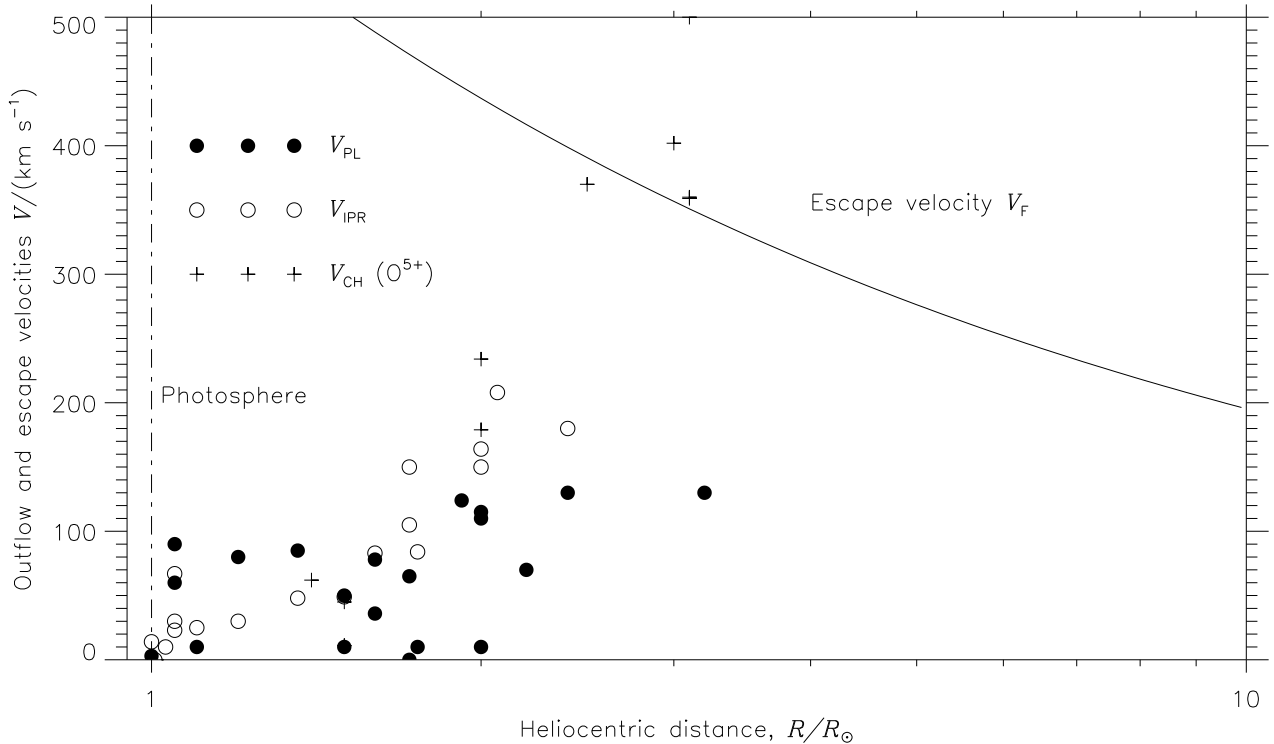


Fig. 2 Flow speeds observed in polar coronal holes (PCHs). Plume and inter-plume-region (IPR) measurements are plotted separately. The observations in the O VI line emitted by O^{5+} ions refer to a PCH. Also shown is the escape velocity as function of the heliocentric distance (cf., Wilhelm et al. 2011).

inant rôle. Elements with a FIP value of $I_X < 10$ eV are defined as low-FIP elements and those with FIP of $I_X > 10$ eV as high-FIP elements, separated by the photon energy $h\nu = 10$ eV of the H I Ly α line.

The photosphere is generally assumed to represent the elemental composition of the outer layers of the Sun. This could be confirmed by Sheminova and Solanki (1999) who showed that only a very minor part of the element segregation observed in the outer solar atmosphere seems to take place in photospheric and sub-photospheric layers. Widing and Feldman (1992) found FIP effects in strong plumes, whereas no significant FIP effect was observed in an IPR of a CH (cf., Feldman 1998; Landi 2008). According to Doschek et al. (1998), the Si/Ne abundance ratio in IPRs in CHs is close to the photospheric value at temperatures near 10^6 K. The abundance ratio of magnesium (a low-FIP element) to neon (a high-FIP element) in plumes is enhanced relative to IPRs by factors of 1.5 and 3.5 (Wilhelm and Bodmer 1998; Young et al. 1999). In Fig. 25 of Wilhelm et al. (2011), plume and IPR observations are compiled to characterize the changes in elemental abundances over a PCH. Plumes can clearly be

identified against the IPRs by their high electron densities obtained from the density-sensitive Si VIII (144.6, 144.0) nm ratio and the lower electron temperatures evident in the line ratio of two ionization stages of silicon. Both the low-FIP elements magnesium and sodium are enriched relative to the high-FIP element neon in plumes with respect to IPRs.

Widing and Feldman (2001) have found in active regions (AR) that the confinement time of a plasma is a decisive parameter for abundance variations. A FIP bias of nearly ten was reached after ≈ 6 d. If these findings can be applied to plumes, we would expect confinement times of a day or so—not too different from plume and BP lifetimes of days (e.g., Wang 1998; DeForest et al. 2001a; Wilhelm et al. 2011).

The different elemental compositions of plumes and IPRs thus suggest that plumes in contrast to IPRs provide some kind of containment for the solar plasma for a period of days, in which the FIP effect can operate.

5 Are there plume signatures in the fast solar wind?

If the IPRs are indeed the source regions of the fast SW, no composition changes would be expected in the high-speed streams in accordance with observations of Geiss et al. (1995). Heber et al. (2013) also reached the conclusion that the SW originating in regions of open magnetic field, would probably not contain matter with any significant mass fractionation.

Thieme et al. (1990) identified with the help of plasma and magnetic field data obtained by the two Helios solar probes 41 fast SW streams between 0.3 ua and 1 ua often with a strong anticorrelation between the variations in the gas pressure and the magnetic pressure were found while the total pressure was nearly constant. Ulysses observations (Reisenfeld et al. 1999) of the high-latitude SW have shown that on time scales of less than one day, the polar SW is dominated by pressure balance structures (PBSs). Fluctuations of the plasma β within PBSs appear to be strongly correlated with fluctuations in the helium abundance. The authors suggest an interpretation of the high β portion of PBSs as the SW extensions of polar plumes. However, the abundance of helium (a high-FIP element) should not be enhanced in plumes, if the neon observations are taken into account.

Direct observation of plumes with SOHO instruments have been made up to $15 R_{\odot}$, “where they fade into the background noise” according to DeForest et al. (1997). Very strong plumes could be followed to $30 R_{\odot}$, but beyond that distance there is no clear indication for the presence of plume plasma in the SW (see, e.g., Poletto et al. 1996; DeForest et al. 2001b; Wilhelm et al. 2011).

Microstreams – identified in Ulysses data – have been analysed by Neugebauer et al. (1995), who concluded that these were not to be identified with plumes. The same result was reported by von Steiger et al. (1999), because no significant depletion of the Ne/Mg abundance and charge-state deviation in these structures could be detected.

6 Spectroscopic peculiarities in polar coronal holes

In most of the studies performed with the SUMER instrument on SOHO (Wilhelm et al. 1995), it was noticed that the profiles of the Ne VIII line were of Gaussian shape in QS regions and in the corona above the limb, but exhibited a strong shoulder on the long-

wavelength wing if seen in PCHs on the solar disk¹. Attempts to explain this shoulder by Si I line blends seen in the first order of diffraction (whereas the Ne VIII line is recorded in the second order with the SUMER detector A) were not successful (Damasch et al. 1999; Wilhelm et al. 2000). The conclusion was that two spectral components with a Doppler separation of 34 km s^{-1} were present nearly symmetrically with respect to the rest wavelength, but the nature of these components remained unclear.

The main purpose of this section and the next is to clarify the situation and provide a physical explanation for the Ne VIII profile in PCHs.

The observations re-analysed here have been presented by Hassler et al. (1999); Damasch et al. (1999); Wilhelm et al. (2000). We consider the Ne VIII line profile in Fig. 5 of the latter paper and apply multi-Gaussian fits on them. This line is very weak in PCHs (Fig. 7 of Wilhelm et al. 1998) and, in particular, in regions with high outflow speeds (Fig. 3 of Wilhelm et al. 2000), presumably IPRs. We, therefore, assume that most of the radiation analysed in Fig. 3a stems from bright plumes and not from IPRs.

The results are shown separately in Fig. 3a and b for the PCH and QS regions. They confirm that the QS profile is of a near Gaussian shape. The PCH profile, however, is built up of three components in the 2nd order spectrum: (1) A blue-shifted component (Doppler shift: 19 km s^{-1}) with a relative contribution of $\approx 45 \%$ to the total line radiance; (2) one with a redshift of 15 km s^{-1} and a contribution of 35% ; (3) a component with a blueshift of $\approx 14 \text{ km s}^{-1}$ and a 15% contribution. All Doppler shifts refer, of course, to line-of-sight components. The outflow speeds along the magnetic field lines are approximately a factor of 1.4 higher (see Sect. 3). The weak 15% peak will be attributed to the outflow in the IPRs with about 14 km s^{-1} .

Although several first-order Si I lines blend the Ne VIII line, they do not produce the shoulder (as mentioned above), and can be disregarded here. The redshifted component (the shaded area in Fig. 3a) is therefore difficult to understand and is an important topic of this article. An explanation will be presented in the next section based on a specific plume model.

¹All raw data acquired are in the public domain and can be obtained either from the SOHO Archive or from the SUMER Image Database at www2.mps.mpg.de/projects/soho/sumer/FILE/SumerEntryPage.html (accessed on 16 Dec. 2014).

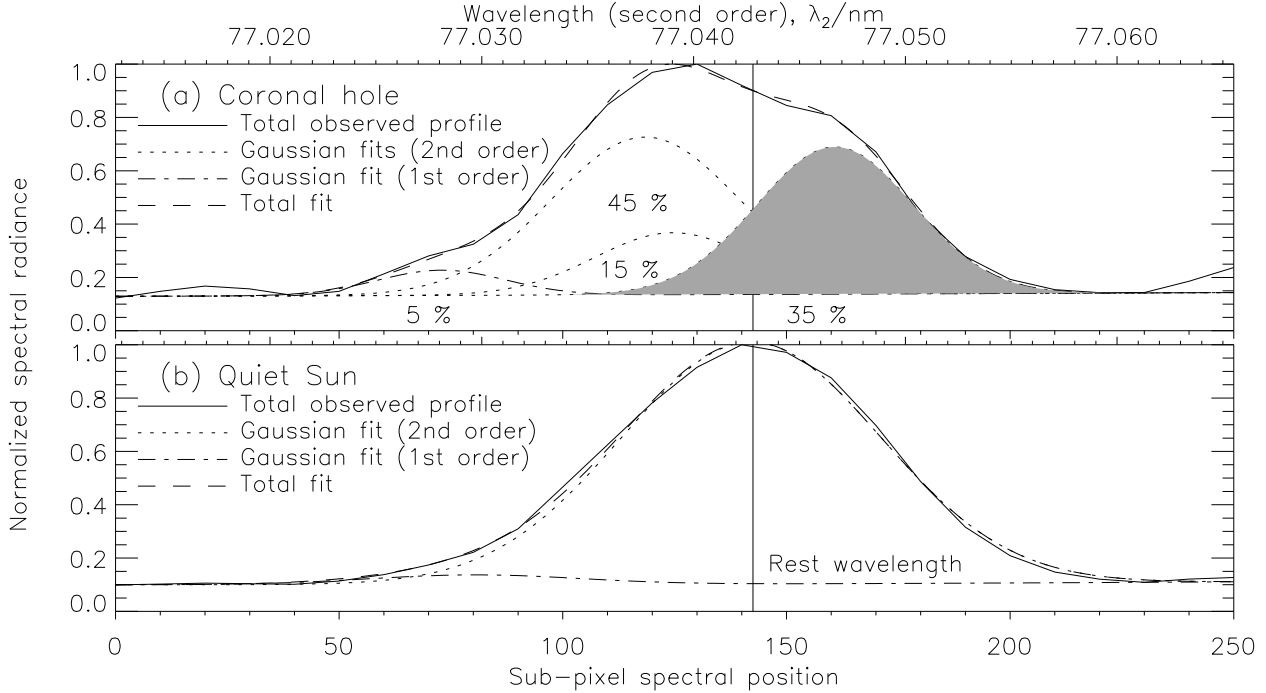


Fig. 3 Spectral profiles covering the Ne VIII line recorded with detector A of SUMER in the second order in a PCH on the solar disk **(a)** and in a QS region **(b)**. The profiles are normalized to one and have been approximated by three Gaussian fits shown in dotted lines for second-order contributions and as dashed-dotted line for a suspected first-order blend of 5 % at 2×77.027 nm. The rest wavelength of the Ne VIII line is indicated at $\lambda_0 = 77.0428$ nm. The total profiles are consistent with a mean blueshift of 6.2 km s^{-1} in PCHs and 0.8 km s^{-1} in QS areas (Damasch et al. 1999). In panel (a) the 45 % peak is shifted to the blue by 19 km s^{-1} , the 15 % peak by $\approx 14 \text{ km s}^{-1}$, and the 35 % peak by 15 km s^{-1} to the red side.

7 Proposed plume model

An outflow velocity of $V_{\text{out}} \approx 300 \text{ km s}^{-1}$ of H^0 is reached in IPRs at $R \approx 3 R_{\odot}$ (Kohl et al. 1998). We will approximate V_{\parallel} , the component parallel to the magnetic field, by V_{out} , and take the transverse velocity, V_{\perp} , also into account in defining the total velocity

$$V = \sqrt{V_{\parallel}^2 + V_{\perp}^2} \quad (3)$$

The Ultraviolet Coronagraph Spectrometer (UVCS) observations on SOHO of $\text{H I Ly } \alpha$ line-width indicate that V_{\perp} of protons is of the order of 200 km s^{-1} at $3 R_{\odot}$, if charge-exchange processes equalize the hydrogen and proton speeds. This gives $V \approx 360 \text{ km s}^{-1}$ and, consequently, most of the material below $\approx 3 R_{\odot}$ is still gravitationally bound to the Sun (cf., also Fig. 2) as long as no post-acceleration is in operation. Such an acceleration depends on waves generated by reconnection processes at or near the footpoints of the funnel (cf., e.g., Ofman 2006).

Given the fact that plumes exist on open magnetic field structures, their geometries are not too different from the magnetic funnels described, e.g. by Tu et al. (2005), for CH regions in general. The first question

is: what are the conditions for a plume formation compared to those for a *normal* funnel? The funnel activity consists of small-scale reconnection events close to the TR and in the low corona. This, in turn, creates heated plasma and waves that are obviously capable of expanding the coronal plasma against gravity and accelerating the fast SW to speeds of $\approx 800 \text{ km s}^{-1}$. One answer could be that such an active funnel at some stage “burns out”. The alternative answer that the activity in a funnel has not yet reached the level required to produce the SW is less likely in view of observed BP/plume evolution sequences (cf., Wang 1998).

Let us now consider how such a shutdown could happen. A narrow funnel interacting with advected small loops will—in addition to generating particle and wave energy—grow through reconnection. However, not all of the advected loops will have the right orientation for a successful interaction. These loops will accumulate around the funnel and might eventually shield it from loops capable of creating reconnection events. This configuration, if visualized in three dimensions, resembles with that of a rosette, a characteristic magnetic feature in the chromospheric network.

The scenario described will not lead to an abrupt shutdown of an active funnel, but to a slow diminution

of the reconnection activity, presumably with the effect that plasma is injected into the funnel without enough post-acceleration to leave the gravitational potential of the Sun. The situation is now comparable to regions on the Sun with closed magnetic field regions – the plasma density will increase and the FIP differentiation would commence. A coronal plume is formed, and at its base a BP might be seen during this phase.

At a later stage, the energy input by reconnection will decrease even more. One could speculate that this is related to the fact that the cross-section of a growing funnel base will increase faster than its circumference. The BP will fade out, but the plume will not immediately collapse under the gravitational pull of the Sun as one might think, even if the thermal energy could be dumped at the base of the plume, which is now assumed to be cool. To show this, we will treat the plasma of the plume in a single-particle approximation, justified by the low density of $n_e \leq 1 \times 10^8 \text{ cm}^{-3}$ (cf., Lie-Svendsen et al. 2002). In a low β regime of a magnetized plasma, the protons will have a magnetic moment that can be written in the non-relativistic case as

$$\mu_p = \frac{[W - m_p U(s)]}{B(s)} \sin^2 \alpha(s), \quad (4)$$

where W is the total proton energy, m_p the proton mass, $U(s)$ the gravitational potential with s a spatial parameter along the field direction, $B(s)$ the magnetic field and the pitch angle, α , defined by

$$\alpha = \arccos \frac{V_{\parallel}}{V}. \quad (5)$$

The magnetic moment will be a constant of the motion, the first adiabatic invariant, as long as Coulomb collisions and wave-particle interactions can be neglected. This concept was first formulated by Alfvén, details of which are described, for instance, by Roederer (1970) for applications in the magnetosphere of the Earth.

If we consider a plume at one of the solar poles, the gravitational potential is

$$U(s) = U(R) = -\frac{G_N M_{\odot}}{R}. \quad (6)$$

Assuming a magnetic pole at $R = 0.56 R_{\odot}$ (cf., Saito 1965), we find a variation of the field in a PCH as

$$B(R) \approx B_0 \left(\frac{R_{\odot}}{R} \right)^{3.6}, \quad (7)$$

where B_0 is the field at the pole. In such a geometry, most of the plasma is trapped. With the assumptions made, it is immediately clear that it cannot leave the

Sun at the upper end of the flux tube. The continuation of the plume flux tube will thus be more or less void of plasma (cf., Wilhelm et al. 2011). At the sunward side only particles within the loss cone will be lost, the others will be mirrored. van de Hulst (1950) demonstrated that the Lorentz force will not influence the hydrostatic equilibrium, but in our configuration it will confine the plume plasma during the radiative cooling phase. During this phase, we would expect plasma flows up and down the plume field lines and suggest that the blue- and red-shifted strong components in Fig. 3a correspond to these flows, if seen along the line of sight.

8 Conclusion

The different elemental compositions of plumes and IPRs strongly suggest that plumes in contrast to IPRs provide some kind of containment for the solar plasma for a period of days, in which the FIP effect can operate.

The continuation of the plume flux tube may be more or less void of plasma (cf., Wilhelm et al. 2011). At the sunward side, only particles within the loss cone will be lost, the others will be mirrored. van de Hulst (1950) demonstrated that the Lorentz force will not influence the hydrostatic equilibrium. In our model, it will confine the plume plasma during the radiative cooling phase. During this phase, we would expect that plasma flows up and down the plume field lines and that the strong blue- and red-shifted components of the neon line correspond to these flows.

We thank the Max-Planck-Institut für Sonnensystemforschung for administrative support and an anonymous referee for constructive comments. The SUMER instrument and its operation are financed by the Deutsches Zentrum für Luft- und Raumfahrt (DLR), the Centre National d'Etudes Spatiales (CNES), the National Aeronautics and Space Administration (NASA), and the European Space Agency's (ESA) PRODEX programme (Swiss contribution). The instrument is part of ESA's and NASA's SOHO mission. This research has made extensive use of the Astrophysics Data System (ADS).

References

- Antonucci, E., Dodero, M.A., Giordano, S., Krishnakumar, V., & Noci, G. 2004, *Astron. Astrophys.*, 416, 749
- Banaszkiewicz, M., Axford, W.I., & McKenzie, J.F. 1998, *Astron. Astrophys.*, 337, 940
- Brekke, P., Hassler, D.M., & Wilhelm, K. 1997, *Sol. Phys.*, 175, 349
- Chae, J., Yun, H.S., & Poland, A.I. 1997, *Astrophys. J. Suppl. Ser.*, 114, 151
- Dammasch, I.E., Wilhelm, K., Curdt, W., & Hassler, D.M. 1999, *Astron. Astrophys.*, 346, 285
- DeForest, C.E., Hoeksema, J.T., Gurman, J.B., et al. 1997, *Sol. Phys.*, 175, 393
- DeForest, C.E., Lamy, P.L., & Llebaria, A. 2001a, *Astrophys. J.*, 560, 490
- DeForest, C.E., Plunkett, S.P., & Andrews, M.D. 2001b, *Astrophys. J.*, 546, 569
- Delaboudinière, J.-P., Artzner, G.E., Brunaud, J., et al. 1995, *Sol. Phys.*, 162, 291
- Doschek, G.A., Feldman, U., & Bohlin, J.D. 1976, *Astrophys. J.*, 205, L177
- Doschek, G.A., Laming, J.M., Feldman, U., et al. 1998, *Astrophys. J.*, 504, 573
- Fawcett, B.C., Jones, B.B., & Wilson, R. 1961, *Proc. Phys. Soc.*, 78, 1223
- Feldman, U. 1998, *Space Sci. Rev.*, 85, 227
- Gabriel, A.H. 1976, *Phil. Trans. R. Soc. London, Ser. A*, 281, 339
- Gabriel, A.H., Bely-Dubau, F., & Lemaire, P. 2003, *Astrophys. J.*, 589, 623
- Gabriel, A., Bely-Dubau, F., Tison, E., & Wilhelm, K. 2009, *Astrophys. J.*, 700, 551
- Geiss, J., Gloeckler, G., & von Steiger, R. 1995, *Space Sci. Rev.*, 72, 49
- Hassler, D.M., Rottman, G.J., & Orrall, F.Q. 1991, *Astrophys. J.*, 372, 710
- Hassler, D.M., Dammasch, I.E., Lemaire, P., et al. 1999, *Science*, 283, 810
- Heber, V.S., McKeegan, K.D., Bochsler, P., et al. 2013, *Lunar Planet. Inst.*, 44, 3028
- van de Hulst, H.C. 1950, *Bull. Astron. Inst. Netherlands*, 11, 150
- Ito, H., Tsuneta, S., Shiota, D., Tokumaru, M., & Fujiki, K. 2010, *Astrophys. J.*, 719, 131
- Kohl, J.L., Noci, G., Antonucci, E., et al. 1998, *Astrophys. J.*, 501, L127
- Landi, E. 2008, *Astrophys. J.*, 685, 1270
- Lie-Svendsen, Ø., Hansteen, V.H., Leer, E., & Holzer, T.E. 2002, *Astrophys. J.*, 566, 562
- McComas, D.J., Barraclough, B.L., Funsten, H.O., et al. 2000, *J. Geophys. Res.*, 105, 10 419
- Neugebauer, M., Goldstein, B.E., McComas, D.J., Suess, S.T., & Balogh, A. 1995, *J. Geophys. Res.* 100, 23 389
- Newkirk, Jr., G., & Harvey, J. 1968, *Sol. Phys.*, 3, 321
- Ofman, L. 2006, *Adv. Space Res.*, 38, 64
- Pasachoff, J.M., Rušin, V., Druckmüller, M., et al. 2009, *Astrophys. J.*, 702, 1297
- de Patoul, J., Inhester, B., Feng, L., & Wiegmann, T. 2013, *Sol. Phys.*, 283, 207
- Peter H., & Judge, P.G. 1999, *Astrophys. J.*, 522, 1148
- Poletto, G., Parenti, S., Noci, G., et al. 1996, *Astron. Astrophys.*, 316, 374
- Raouafi, N.-E., & Stenborg, G. 2014, *Astrophys. J.*, 787, 118
- Raouafi, N.-E., Petrie, G.J.D., Norton, A.A., Henney, C.J., & Solanki, S. K. 2008, *Astrophys. J.*, 682, L137
- Reisenfeld, D.B., Mc Comas, D.J., & Steinberg, J.T. 1999, *Geophys. Res. Lett.*, 26, 1805
- Roederer, J.G. 1970, *Dynamics of geomagnetically trapped radiation*, (Springer-Verlag, Berlin, Heidelberg, New York)
- Saito, K. 1965, *Publ. Astron. Soc. Japan*, 17, 1
- Sheeley, Jr., N.R., Wang, Y.-M., Hawley, S.H., et al. 1997, *Astrophys. J.*, 484, 472
- Sheminova, V.A., & Solanki, S.K. 1999, *Astron. Astrophys.*, 351, 701
- von Steiger, R., Fisk, L.A., Gloeckler, G., Schwadron, N.A., & Zurbuchen, T.H. 1999, *AIP Conf. Proc.*, 471, 143
- Thieme, K.M., Marsch, E., & Schwenn, R. 1990, *Ann. Geophys.* 8, 713
- Tu, C.-Y., Zhou, C., Marsch, E., et al. 2005, *Science*, 308, 519
- Wang, Y.-M. 1998, *Astrophys. J.*, 501, L145
- Widing, K.G., & Feldman, U. 1992, *Astrophys. J.*, 392, 715
- Widing, K.G., & Feldman, U. 2001, *Astrophys. J.*, 555, 426
- Wilhelm, K. 2006, *Astron. Astrophys.*, 455, 697
- Wilhelm, K., & Bodmer, R. 1998, *Space Sci. Rev.*, 85, 371
- Wilhelm, K., Curdt, W., E. Marsch, E., et al. 1995, *Sol. Phys.*, 162, 189
- Wilhelm, K., Lemaire, P., Dammasch, I.E., et al. 1998, *Astron. Astrophys.*, 334, 685
- Wilhelm, K., Dammasch, I.E., Marsch, E., & Hassler, D.M. 2000, *Astron. Astrophys.*, 353, 749
- Wilhelm, K., Inhester, B., & Newmark, J.S. 2002, *Astron. Astrophys.*, 382, 328
- Wilhelm, K., Abbo, L., Auchère, F., et al. 2011, *Astron. Astrophys. Rev.*, 19, 35
- Woch, J., Axford, W.I., Mall, U., et al. 1997, *Geophys. Res. Lett.*, 24, 2885
- Young, P.R., Klimchuk, J.A., & Mason, H.E. 1999, *Astron. Astrophys.*, 350, 286